Reliability-Based Calibration of the Slenderness Limit of Concrete Columns Reinforced with GFRP Bars for CSA S6 and CSA S806

Koosha Khorramian[1], Fadi Oudah[2], and Pedram Sadeghian[3]

[1] Department of Civil and Resource Engineering, Dalhousie University, 1360 Barrington Street, Halifax, NS, B3H 4R2 Canada, Email: koosha.khorramian@dal.ca **(Corresponding author)**

[2] Department of Civil and Resource Engineering, Dalhousie University, 1360 Barrington Street, Halifax, NS, B3H 4R2 Canada Email: fadi.oudah@dal.ca

[3] Department of Civil and Resource Engineering, Dalhousie University, 1360 Barrington Street, Halifax, NS, B3H 4R2 Canada, Email: pedram.sadeghian@dal.ca

Competing interests: The authors declare there are no competing interests.

ABSTRACT:

The design provisions for internal glass fiber-reinforced polymer (GFRP) reinforced concrete (RC) columns have recently been under consideration by design committees in Canada and around the world due to new advancements in the understanding of the behavior of GFRP-RC columns. The design considerations require optimized and reliable calibration of the design parameters. The slenderness limit is a critical design parameter differentiating between the first-order and second-order analyses of GFRP-RC columns. The existing slenderness limits in design standards were calibrated using deterministic approaches. In this study, a novel reliability-based approach was utilized to quantify the reliability index associated with the slenderness limit to calibrate the slenderness limit for CSA S806 and CSA S6, for the first time. The method takes the advantage of artificial intelligence (AI) and incorporates a comprehensive experimental database. This study recommends optimized reliable slenderness limit equations for GFRP-RC columns for CSA S806 and CSA S6.

KEYWORDS:

Code Calibration; Reliability analysis; Slenderness Limit; Concrete Columns; GFRP Bars; Artificial Neural Network; Second-Order Analysis.

INTRODUCTION

The use of glass fiber-reinforced polymer (GFRP) bars in concrete structures have become an effective solution to avoid corrosion in a harsh environment. The increasing demand for GFRP bars in the industry led to extensive research programs in the past decade (Abdelazimet al 2020a; Abdelazim et al 2020b; Barua et al. 2021; Barua and El-Salakawy 2020; Hales et al. 2016; Hasan et al. 2017; Kharal and Sheikh 2020; Khorramian and Sadeghian 2020). Also, the design considerations for GFRP-reinforced concrete (RC) structures are being actively included in design guidelines such as CSA S806-12 (CSA 2017), CSA S6-19 (CSA 2019), and ACI 440.1R-15 (ACI Committee 440 2015).

The design of concrete columns reinforced using GFRP has been historically treated with caution due to the lack of experimental evidence when FRP design guidelines were first developed. However, the increasing number of experimental studies on the behavior of GFRP-RC columns has contributed to gradually relaxing the stringent guidelines related to GFRP RC column design (Afifi et al. 2014; Guérin et al. 2018a; Guérin et al. 2018b; Hadhood et al. 2016; Hadhood et al. 2017; Khorramian and Sadeghian 2017; Mohamed et al. 2014; Tobbi et al. 2012). For example, CSA S6-19 (CSA 2019) allows a strain of up to 0.002 mm/mm for GFRP bars in compression while its contribution was neglected in previous versions. The CSA S806-12 (CSA 2017) allows the use of GFRP bars for short columns while the use of GFRP bars in compression was not recommended in the previous versions. Moreover, in the upcoming ACI 440 code, the design of slender GFRP-RC columns is being considered for the first time in a design code, which emphasizes the improvements and acceptance of GFRP bars in compression and slender columns. Therefore, design parameters such as the slenderness limit are required to be investigated. The slenderness limit defines the required analysis type and categorizes the columns into short and slender columns. For short concrete columns, first-order analysis is adequate, while for slender columns, second-order analysis is required.

For steel-RC columns, CSA A23.3-19 (CSA 2019) requires designers to consider second-order analysis for slender columns, defined as columns with a slenderness ratio that is greater than the slenderness limit presented in Eq. [1].

[1] $$\lambda_{cr} = \frac{25-10(M_1/M_2)}{\sqrt{\frac{P_f}{A_g f_c}}}$$

where λ_{cr} is slenderness limit, M_1 and M_2 are the column end moments (M_2 has the largest magnitude), M_1/M_2 is the end moment ratio which is positive for single curvature and negative for double curvature columns, P_f is the factored load, A_g is the gross cross-section area, and f_c is the concrete strength. It is seen from Eq. [1] that the slenderness limit is a function of factored load and can vary by changing the factored load P_f. On the other hand, for steel-RC columns, CSA S6-19 (CSA 2019) recommends the use of a constant slenderness limit for all cross-sections, material properties, and load levels, as presented in Eq. [2].

[2] $$\lambda_{cr} = 34 - 12(M_1/M_2) \leq 40$$

For GFRP-RC columns, CSA S806-12 (CSA 2017) adopts Eq. [2] and sets it as the slenderness limit. However, it does not allow the use of slender GFRP-RC columns and states that only columns with slenderness ratios less than Eq. [2] are allowed to be used. It should be mentioned that Eq. [2] was originally developed by MacGregor et al. (1970) and is currently being used in ACI 318-19 (2019). Since Eq. [2] is developed for steel-RC columns, complementary studies are required to confirm the adequacy of this slenderness limit for GFRP-RC columns because of the difference between the mechanical properties of GFRP bar and steel rebar. It is well-known that GFRP bars have a much lower modulus of elasticity than steel rebar, which is likely to make GFRP-RC columns susceptible to larger second-order deformation than their counterparts reinforced with steel rebar. Also, steel rebar yields as the strain increase either in compression or tension while GFRP bars either rupture in tension or crush in compression. As a result, the modes of failure of GFRP-RC columns and steel-RC columns are different. Moreover, the statistical characteristics of steel rebar and GFRP bars are different, which leads to a different level of uncertainty of the slenderness limit for GFRP-RC columns compared to steel-RC columns. Independent calibration is required for each design standard irrespective of the similarities in material properties. This is because the input load statistics and design equations differ among design standards. For example, the calibration of the slenderness limit for CSA S806 would be distinct from the one in CSA S6. Thus, these reasons constitute the motivation of the current research which is related to proposing reliability-based optimized slenderness limits for GFRP-RC columns.

Mirmiran et al. (2001) conducted a numerical and statistical analysis for GFRP-RC columns and proposed a slenderness limit of 17 for columns bent in symmetric single curvature. A 5% drop in axial capacity of GFRP-RC columns calculated based on a second-order and first-order analysis was the defining criterion for the study, which was adopted from MacGregor et al. (1970). Zadeh and Nanni (2013) adopted the proposed slenderness limit of 17 and shifted Eq. [2] to start at this limit for the symmetric single curvature case. Later, Zadeh and Nanni (2017) proposed another slenderness limit equation based on an analytical approach by setting a magnification factor equal to 1.14, which corresponds to a 5% drop criterion for high levels of axial loads. Zadeh and Nanni (2017) also proposed a modification factor to their proposed slenderness limit which is a function of concrete strength and it applies to the slenderness limit of sections built with high strength concrete. Abdelazim et al. (2020c) also proposed a slenderness limit for GFRP-RC columns based on a 5% drop criterion utilizing an experimental and analytical approach. The study suggested a slenderness limit of 18 and shifted the slenderness limit shown in Eq. [2] to start from 18 for the single curvature case. Recently, for the first time, Khorramian et al. (2021c) proposed a reliability-based approach instead of using the 5% drop approach for quantifying the safety margin of the slenderness limit of GFRP-RC columns based on ACI's load and strength factors. The approach enables the incorporation of the experimental database, quantification of the reliability index of the slenderness limit, and optimization of the slenderness limit for code calibration purposes.

There is an existing research gap related to quantifying the current slenderness limit for GFRP-RC columns in CSA S806-12 (CSA 2017) and a lack of optimized slenderness limit for CSA S806 and CSA S6 standards. Therefore, the objective of this study is to propose new slenderness limits for GFRP-RC columns for CSA S806 and CSA S6 based on a novel reliability-based approach. In the following sections, the novel reliability-based methodology is explained.

RESEARCH SIGNIFICANCE

The slenderness limits for RC columns in CSA S806 and CSA S6 are based on a deterministic approach considering a 5% drop of axial load between first-order and second-order analyses. A novel reliability-based approach is employed in this research to propose slenderness limit equations for concrete columns reinforced using GFRP bars to achieve predefined target safety limits consistent with the respective design standards. The novel approach utilized artificial intelligence (AI) and reliability analysis.

ANALYSIS FRAMEWORK

The reliability analysis, implemented in this study, is a combination of Monte Carlo simulation (MCS) and first-order reliability method (FORM) with modifications suggested by Rackwitz and Fiessler (Rackwitz and Flessler 1978; Nowak and Collins 2000) to consider the distribution types, called FROM-RF in this paper. The method requires building the resistance distributions using MCS and finding the reliability index with resistance and loads distributions.

Reliability Analysis

The slenderness limit determines whether the column can be designed based on a first-order (for short columns) or second-order analysis (for slender columns). Therefore, the reliability analysis can be conceptualized to assess the safety by addressing the following principal question: what is the probability of failure of a column if it is designed based on a first-order factored resistance but fails under the design loads if the secondary moment effects are considered as the unfactored resistance (using a second-order analysis modified with the experimental database as presented in Fig. 1(a))? By selecting a slenderness ratio as the slenderness limit, for a number of cases with different design parameters (called design space), the reliability index can be found quantitatively by addressing the aforementioned principal question using a reliability-based procedure as presented in Fig. 1(b). The reliability procedure was conducted in three stages as depicted in Fig. 1(b): 1) determination of the mean value of the loads; 2) building the resistance distribution; 3) conducting FORM-RF to find the reliability index.

The reliability analysis in this study is only concerned with applied dead and live loads since the design of RC columns is typically governed by gravity loads. To determine the mean of loads, the nominal value of loads should be calculated first. The nominal value of the loads for a given dead-to-live load ratio (*D/L*) can be found by satisfying the design equation and setting the factored load equal to the factored resistance (i.e., demand-to-capacity ratio equals 1.0), as presented in Eq. [3].

[3] $$P_r = P_f$$

where P_r is the factored resistance and P_f is the factored load. For the calibration of CSA A23.3 and CSA S806, P_f can be found using Eq. [4] and Eq. [5] per NBCC (NBCC 2015).

[4] $$P_f = 1.25P_D + 1.5P_L$$

[5] $$P_f = 1.4P_D$$

where P_D is the nominal dead load and P_L is the nominal live load. For the calibration of CSA S6, P_f can be calculated using Eq. [5] and Eq. [6].

[6] $$P_f = 1.2P_D + 1.7P_L$$

The factored resistance is calculated per corresponding Canadian standard for steel-RC columns (CSA A23.3-19 2019; CSA S6-19 2019) and GFRP-RC columns (CSA S806-12 2017; CSA S6-19 2019). The factored interaction diagram is shown in Fig. 1(a) where the maximum compressive strain is 0.0035 mm/mm (i.e., ε_{cu} = 0.35%), the concrete resistance factor is 0.65 (i.e., ϕ_c = 0.65) per CSA A23.3-19 (CSA 2019), the steel resistance factor is 0.85 (i.e., ϕ_s = 0.85) per CSA A23.3-19 (2019) and CSA S6-19 (CSA 2019), the GFRP resistance factor is 0.75 (i.e., ϕ_f = 0.75) per CSA S806-12 (CSA 2017) or 0.65 (i.e., ϕ_f = 0.65) per CSA S6-19 (CSA 2019), while concrete in tension is neglected. It is noted that the GFRP resistance factor specified in CSA S6-19 is a product of a reliability-based material factor (0.8) and a regression-based environmental factor. The reliability evaluation of the slenderness limit presented in this study is concerned with the material factor (0.8) since it is a reliability-based factor that accounts for the variance in the material response (i.e., it is definition is consistent with the material resistance factor definition adopted by Canadian standards). Also, as a complementary to this study, separate calculations were conducted for a resistance factor of 0.65 for comparison purposes only. More details on resistance and load statistics can be found in the referenced study (Oudah and Hassan 2021).

By performing the first-order analysis using the factored interaction diagram and setting the factored load equal to the factored resistance, the nominal dead and live loads for a given D/L can be found, as presented schematically in Fig. 1. The nominal values are multiplied by their corresponding bias to obtain the mean value of the load distributions for the reliability analysis.

The resistance distribution can be found using MCS by considering the resistance model discussed in the following section. To achieve this, seven random variables were considered for the MCS including concrete strength (f_c), yield stress of steel (f_y), tensile strength of GFRP bars (f_{fcu}), compressive strength of GFRP bars (f_{ftu}), depth of bars in compression (d_c), depth of bars in tension (d_t), and the ratio of the finite-difference model to the experimental database (ψ_{FE}). One thousand randomly generated trials were sampled from the seven input distributions. The randomly generated inputs were fed into the resistance model to build the distribution of the resistance, as shown in the right branch of the analysis procedure in Fig. 1(b). It should be highlighted that the distribution of resistance is lognormal for both GFRP-RC columns and steel-RC columns. Therefore, the resistance distribution was considered as a lognormal distribution with a mean and a standard deviation determined from the MCS conducted with the resistance model and the seven random variables.

The performance function of the limit state is expressed in Eq. [7].

[7] $$g = R - L'$$

where g is the performance function, R is the resistance, and L' is the load. As some of the distributions of loads and resistance are non-normal, FORM-RF (Rackwitz and Flessler 1978; Nowak and Collins 2000) was utilized to calculate the reliability indexes. In FORM-RF, the random variables are transformed to their equivalent normal distributions using Eq. [8] to [10].

[8] $$\boldsymbol{Z}^* = [Z_1^* \, Z_2^* \ldots Z_n^*]^T; \; Z_i^* = \frac{X_i^* - \mu_{X_i}^e}{\sigma_{X_i}^e}$$

[9] $$\mu_{X_i}^e = X_i^* - \sigma_{X_i}^* \left[\Phi\left(F_X(X_i^*)\right)\right]$$

[10] $$\sigma_{X_i}^e = \frac{1}{f_X(X_i^*)} \phi\left(\Phi^{-1}\left(F_X(X_i^*)\right)\right)$$

where $\boldsymbol{Z}^*$ is a vector of normalized design points, Z_i^* is the i^{th} normalized design point corresponding to the i^{th} non-normal design point X_i^*, $\mu_{X_i}^e$ and $\sigma_{X_i}^e$ are the mean and standard deviation of the equivalent normal distribution for the i^{th} random variable, respectively, ϕ and Φ are the probability density function (PDF) and the cumulative distribution function (CDF) of standard normal distribution, respectively, Φ^{-1} is the inverse CDF of the standard normal distribution, and $f_X(X_i^*)$ and $F_X(X_i^*)$ are the PDF and CDF of X_i^*, respectively. It should be noted that the design point is the most probable point (MPP) whose distance from the origin of the standard normal space is minimized, called the Hasofer-Lind reliability index (Nowak and Collins 2000). To find the reliability index, a linear approximation of the performance function is fitted at the design point to the performance function to find the Hasofer-Lind reliability index (β) with an iterative procedure. More details on performing FORM-RF can be found in the corresponding references (Rackwitz and Flessler 1978; Nowak and Collins 2000).

Resistance Model

The resistance model is derived by incorporating an experimental database and finite difference method (FDM) in the form of an artificial neural network (ANN) analysis with two modification random variables as presented in Eq. [11].

[11] $$R = \frac{F_{ANN}}{\Psi_{AF}\Psi_{FE}}$$

where R is the resistance of a column, F_{ANN} is the second-order axial capacity of the studied column, ψ_{AF} is a random variable defined as the ratio of second-order analysis performed by ANN to FDM, and ψ_{FE} is a random variable defined as the ratio of FDM to experimental capacity.

The ANN is recognized as a viable analysis method in the literature (Ahmad et al. 2021; Raza et al.2020; Malakzadeh and Daei 2020; Naderpour et al. 2018). Particularly, ANN was used to analyze the capacity of short GFRP-RC columns (Raza et al. 2020), and to perform reliability analysis for short GFRP-RC columns (Ahmad et al. 2021). In this study, the second-order ANN model developed by Khorramian et al. (2021a) was adapted. The ANN was built by training a network with 2,915,000 grids of FDM analysis for GFRP-RC columns with eleven analysis parameters. The FDM method considers the nonlinearity in material and geometry and was verified against experimental tests. To train the ANN an optimized configuration for second-order analysis was used consists of three hidden layers with 35, 30, and 15 neurons, sigmoid activation function, and Levenberg-Marquardt backpropagation algorithm were used for the ANN. The comparison of the ANN versus FDM revealed a coefficient of determination of 1 (i.e., R^2=1) and a root mean squared error of 1 kN (i.e., RMSE = 1kN) showed a very good agreement between the ANN and FDM analysis for almost 3 million FDM analyses. More details on the optimized ANN modeling and training can be found in the referenced study (Khorramian et al. 2021a).

The ratio of ANN to FDM (ψ_{AF}) showed a normal distribution with a mean of 1.0 and a coefficient of variation (COV) of 0.00085 for GFRP-RC columns, and a mean of 1.0 and a COV of 0.00054 for steel-RC columns. Therefore, for the reliability analysis, ψ_{AF} was considered as a deterministic parameter. To incorporate the experimental database, 85 eccentrically loaded GFRP-RC and 102 steel-RC column tests were collected from the literature (Elchalakani et al. 2019; Elchalakani and Ma 2017; Elchalakani et al. 2018; Guérin et al. 2018a; Guérin et al. 2018b; Hadi and Youssef 2016; Hognestad 1951; Khorramian and Sadeghian 2017; Khorramian and Sadeghian 2020; Kim and Yang 1995; Salah-Eldin et al. 2019; Salah-Eldin et al. 2020; Sun et al. 2017; Xue et al. 2018). The ratio of FDM to experimental capacities (ψ_{FE}) showed a lognormal distribution with a mean of 1.10 and a coefficient of variation (COV) of 0.14 for GFRP-RC columns, and a mean of 1.04 and a COV of 0.10 for steel-RC columns. Therefore, for reliability analysis, ψ_{FE} in Eq. [11] was considered as a random variable. The statistical parameters of the resistance model including distribution type, bias, and COV can be found in Table 1.

Load Model

The load L' in Eq. [7] is obtained using Eq. [12].

[12] $$L' = P'_D + P'_L \times P'_{LT}$$

where P'_D is the axial dead load, P'_L is the axial live load, and P'_{LT} is the transformation to live load effect. It should be mentioned that dead, live, and transformation to live load in Eq. [12] are not nominal values, instead, they can take any random value from their corresponding distributions. For MCS, the distribution of load components is built with the mean value found by the reliability approach explained earlier and for each MCS trial, a random load is selected from the distributions to be compared with a randomly selected resistance. The statistical parameters of the load model including distribution type, bias, and COV can be found in Table 1. Load statistics used for calibrating the slenderness limits for CSA S6 in CSA S806 were based on traffic loads used in calibrating CSA S6 and building loads used in calibrating the National Building Code of Canada (NBCC). This was followed to ensure consistency in the calibration process since loads used for the design of a pier following CSA S6 are specified in the same code itself, while loads used for the design of a column following CSA S806 are specified in NBCC.

PARAMETRIC STUDY

The developed reliability method is utilized to conduct a parametric study concerning the influential design parameters to quantify the reliability of the slenderness limits included in the current standards for steel-RC columns as a reference (i.e., CSA A23.3 and CSA S6), and to propose new optimized slenderness limits for GFRP-RC columns, calibrated for CSA S806 and CSA S6.

To conduct the parametric study, a design space including 291,600 and 194,400 cases for GFRP-RC and steel-RC columns were considered, respectively, as shown in Table 2. Eight design parameters were considered for steel-RC and GFRP-RC columns in the design space (see Table 2). For GFRP-RC columns, 291,600 cases were divided into three groups to study GFRP-RC columns based on design consideration and load statistics for CSA S806 with GFRP resistance factor of 0.75 (97,200 cases), CSA S6 with GFRP resistance factor of 0.8 (97,200 cases), and CSA S6 with GFRP resistance factor of 0.65 (97,200 cases). It should be mentioned that the number of studied cases is reduced to cover only effective design parameters, as a previous study by the authors (Khorramian et al. 2021c) revealed that the parameters in Table 2 are the most effective in the reliability analysis of the slenderness limit. The reliability procedure explained in the previous section was utilized for all cases in Table 2 and a total of 486,000 reliability indexes were determined.

The result of the parametric study is shown in Fig. 2(a) for GFRP-RC columns and Fig. 2(b) for steel-RC columns with statistics and resistance factor of CSA S806 and CSA A23.3, respectively. To interpret the results, the effect of the parameters on both first-order and second-order analyses should be considered simultaneously. For both GFRP-RC columns and steel-RC columns, the results revealed that as concrete strength increases, the reliability index decreases. This trend can be explained by the fact that the factored first-order capacity increases as the concrete strength increases, which causes an increase in the mean of applied loads that were considered for the reliability analysis. Meanwhile, the secondary moment effect decreases as the concrete strength increases since the modulus of elasticity of concrete increases and deflection of column decreases. However, the results revealed that the increase in the mean of loads is dominant compared to the increase in the second-order capacity, which leads to a total reduction in the reliability index. Also, the results showed that as the eccentricity ratio increases, the reliability index decreases for GFRP-RC and steel-RC columns because the secondary moment effect is amplified as the flexural load increases. It was observed that for GFRP-RC columns with double curvature, the reliability index for eccentricity ratios of 0.1 and 0.3 converges, which means the first-order analysis (and in turn the mean of loads) becomes dominant.

For GFRP-RC columns, the variation in other parameters such as reinforcement depth ratio, reinforcement ratio, and modulus of elasticity of FRP bars showed a slight variation in the reliability index, which indicates the marginal impact of these parameters on the reliability. For steel-RC columns, as the reinforcement depth ratio increases, the reliability index increases. Also, as reinforcement ratio and yield stress for steel-RC columns increase, the reliability index decreases.

The reliability index for different slenderness limits is presented in Fig. 2(c) through Fig. 2(f). For all studied cases, it is observed that as the slenderness limit increases, the reliability index decreases, which means the selection of lower slenderness limits would help in increasing the safety margin. Moreover, as expected, due to less variability in steel characteristics compared to GFRP bars, it was observed that the reliability indexes are higher for steel-RC columns compared to GFRP-RC columns, as shown in Fig. 2. The results also reveal that as the end moment ratio (M_1/M_2) varies from single curvature to double curvature, the reliability index increases. The latter can be justified by the fact that the larger moment governs the design for a column with different end moments while the second-order analysis considers the variation of the moment profile along with the column height. As a result, the higher second-order capacity (and the resistance) become more dominant for the reliability analysis for columns with different end eccentricities.

The results revealed that for the steel-RC columns considered for CSA A23.3 (Fig. 2(c)) and the GFRP-RC columns considered for CSA S806 (Fig. 2(e)), as dead to dead plus live load ratios, $D/(D+L)$, increases from zero to one, the reliability index increases and reaches a peak at first, then it decreases to a minimum of 0.9 and increases again to reach 1.0. For GFRP-RC columns considered for CSA S6 with a GFRP resistance factor of 0.8 (fig. 2(d)), as $D/(D+L)$ increases from zero to one, the reliability decreases to reach 0.9, then it increases to 1. For steel-RC columns considered for CSA S6 (fig. 2(f)), similar behavior to GFRP-RC columns (Fig. 2(d)) was observed with the difference that the rate of decrease is higher from $D/(D+L)$ of 0 to 0.2. It should be mentioned that these differences are attributed to different design considerations, load combinations, material statistics, and resistance factors corresponding to each design standard.

For the calibration of resistance factor for GFRP-RC bending members, a range of live-to-dead load ratio (*L*/*D*) of 1 to 3 were studied in the literature (Shield et. al 2011) which corresponds to *D*/(*D*+*L*) of 0.25 to 0.5. A recent survey based on actual measurements of office loads showed a *D*/*L* of 4 for office buildings (Oudah et. al 2019), which is equal to *D*/(*D*+*L*) of 0.8. With the observed trend in *D*/(*D*+*L*) and comparing to the recent studies, a range of 0.25 to 0.8 for *D*/(*D*+*L*) was considered in this study. The lowest values of the reliability index in this range were corresponding to *D*/(*D*+*L*) of 0.8 for all studied design standards. Therefore, a *D*/(*D*+*L*) ratio of 0.8 is considered in this study for the reliability evaluation and calibration in the following section.

RELIABILITY EVALUATIONS

To evaluate the existing equations for slenderness limit and to propose new customized slenderness limits for CSA S806 and CSA S6, the reliability indexes corresponding to the whole database (i.e., cases in Table 2) were considered for the reliability analysis. For CSA A23.3-19 (CSA 2019), the equivalent slenderness limit (λ_{eq}) was built based on Eq. [13] to evaluate the reliability index associated with Eq. [1], as shown in Fig. 3(a).

[13] $$\lambda_{eq} = \lambda_{cr}\sqrt{\frac{P_f}{A_g f_c}}$$

The evaluation of the slenderness limit in Eq. [2] for steel-RC columns per CSA S6-19 (2019) is shown in Fig. 3(b). The analysis showed that the reliability index varies between 4.18 to 5.32 and between 4.42 to 4.64 for CSA A23.3-19 equation (CSA 2019) and CSA S6-19 (CSA 2019) equations, respectively. The lowest reliability is corresponding to the symmetric single curvature case, and it increases by moving to double curvature, which is compatible with the code equations to allow higher values for the slenderness limits in double curvature cases.

For GFRP-RC columns, Eq. [2] was evaluated for CSA S806-12 (CSA 2017) using the cases with GFRP resistance factor of 0.75 (i.e., ϕ_f = 0.75), as presented in Fig. 4(a). The results reveal that the reliability index varies between 3.94 to 4.63 by moving from single curvature to double curvature cases. It is seen that the reliability indexes are lower for GFRP-RC columns than the steel-RC columns. Therefore, further considerations may be required to provide an acceptable level of safety for GFRP-RC columns. A study by Szerszen and Nowak (2003), which formed the basis for calibrating the load and reduction factors in ACI 318-19 (2019), recommends a target reliability index of 4.0 for reinforced concrete columns. Therefore, a target reliability index of 4.0 was adopted to calibrate the slenderness limit for GFRP-RC columns in this study. The proposed slenderness limit equation for CSA S806 was calibrated to meet a target reliability index of 4.0 for the symmetric single curvature case, linearly varying to reach the slenderness limit of 40 at an end moment ratio of -0.5 (M_1/M_2 = -0.5), while capping the slenderness limit at 40, as presented in Fig. 4(b). For the proposed equation, the reliability index varies between 4.00 to 4.63 by moving from single curvature to double curvature. The proposed equation for the slenderness limit of CSA S806 is presented in Eq. [14], which starts with a slenderness limit of 20.5 for symmetric single curvature GFRP-RC columns.

[14] $\lambda_{cr} = 33.5 - 13(M_1/M_2) \leq 40$

For GFRP-RC columns designed based on CSA S6, the proposed slenderness limit is evaluated using the GFRP resistance factor of 0.8 and 0.65 (i.e., two separate analyses were conducted). Please refer to the Introduction section of this paper for more discussion regarding the difference between the 0.8 and 0.65 factors. For the analysis with GFRP resistance factor of 0.8, the slenderness limit corresponding to target reliability of 4.00 was found as 21.85 which was rounded up to 22 with a reliability index of 3.9942. The latter is compatible with the conventional format of the slenderness limit for steel-RC columns (i.e., Eq. [2]), which is proposed to be used for GFRP-RC columns designed per CSA S6 with a reliability range of 3.99 to 4.75, as presented in Fig. 4(c) and Eq. [15].

[15] $\lambda_{cr} = 34 - 12(M_1/M_2) \leq 40$

For assessing the slenderness limit for CSA S6, if a GFRP resistance factor of 0.65 is used instead of 0.8, the reliability index corresponding to Eq. [15] increases, as presented in Fig. 4(d). The range of reliability index varies from 4.26 to 5.03 for Eq. [15] varying from single curvature to double curvature by considering a GFRP resistance factor of 0.65. By setting the single curvature slenderness limit to 27, a target reliability index of 4.00 can be reached, and the corresponding slenderness limit can be presented in Eq. [16].

[16] $\lambda_{cr} = 35\frac{2}{3} - 8\frac{2}{3}(M_1/M_2) \leq 40$

The reliability index for Eq. [16] varies from 3.99 to 5.03 by moving from single curvature to double curvature columns. By comparing the reliability corresponding to Eq. [15] and Eq. [16], it can be concluded that Eq. [15] is more conservative. Also, by comparing the results of the analysis with GFRP resistance factors of 0.8 and 0.65, it can be concluded that Eq. [15] meets a target reliability index of 4 for both cases. Therefore, this paper recommends the use of Eq. [14] and Eq. [15] as slenderness limits for GFRP-RC columns for CSA S806 and CSA S6, respectively. As a result, for the symmetric single curvature case, the slenderness limits of 20.5 and 22 are recommended for CSA S806 and CSA S6, respectively.

SUMMARY AND CONCLUSION

This study focused on the evaluation and calibration of slenderness limits for GFRP-RC columns for CSA S6 and CSA S806 using a reliability-based approach. This is the first study to propose a slenderness limit based on a holistic reliability assessment as opposed to the traditional deterministic criterion corresponding to a 5% drop of second order to first order column analysis ratio for CSA S6 and CSA S806. The reliability-based approach quantifies the probability of failure of a short column designed based on first-order analysis, for which the short column is categorized based on slenderness limit. The reliability-based approach consists of load and resistance models. The load model was selected to be compatible with the studied standards (i.e., CSA S6 and CSA S806), while the resistance model was the same for all studied cases. For the resistance model, an artificial neural network (ANN) was used as a replacement to the finite difference method (FDM), which was trained by almost 3 million FDM analyses, and further modified to include the experimental database in the resistance model. For the reliability analysis, MCS and FORM-RF methods were utilized to assess the reliability index of 291,600 GFRP-RC columns and 194,400 steel-RC columns with 8 design parameters. The following conclusions are drawn from this study:

- The parametric study showed that the reliability index is sensitive to the input load statistical parameters (distribution type, bias, and coefficient of variation) and the considered load combination. Therefore, the slenderness limits should be separately calibrated for the CSA S806 and CSA S6 based on the corresponding building load statistics and bridge load statistics, respectively, to meet the same target reliability index.
- The parametric study revealed that concrete strength and eccentricity ratio are the most impactful parameters in the calibration of the slenderness limit. As concrete strength increases, the reliability index decreases due to an increase in the first-order capacity and mean of loads which are more effective than the enhanced stiffness associated with the higher concrete strength. As the eccentricity ratio increases, the reliability index decreases due to an increase in the secondary moment effects and an increase in the resistance.

- The results showed that the lowest reliability index is corresponding to symmetric single curvature columns. As the end moment ratio varies from single curvature to double curvature, the reliability index increases because of the difference between first-order and second-order analysis assumptions.
- The reliability index for the slenderness limit of GFRP-RC columns is lower than steel-RC columns as shown by the results of the analysis, which can be attributed to the higher variability of GFRP bars comparing to steel bars.
- The reliability evaluation for steel-RC columns showed a range of 4.18 to 5.32 and 4.42 to 4.63 for reliability index corresponding to the slenderness limits in CSA A23.3 and CSA S6, respectively. For GFRP-RC columns, the code evaluation showed a reliability range of 3.94 to 4.63 for the slenderness limit.
- To calibrate the slenderness limit for GFRP-RC columns, a target reliability index of 4.0 was selected which corresponds to slenderness limits of 20.5 and 22 for CSA S806 and CSA S6 code calibrations for single curvature cases, respectively.
- Eq. [14] and Eq. [15] are proposed to be used as the slenderness limits of GFRP-RC columns for CSA S806 and CSA S6, respectively. Eq. [14] provides a reliability index range of 4.00 to 4.63. Eq. [15] provides a reliability range of 3.99 to 4.75 and 4.25 to 5.03 for GFRP resistance factors of 0.8 and 0.65, respectively.

ACKNOWLEDGEMENT

The authors would like to thank Dalhousie University and the Natural Sciences and Engineering Research Council (NSERC) for supporting this research program.

DATA AVAILABILITY

Some or all data, models, or codes generated or used during the study are available from the corresponding author by request.

REFERENCES

Abdelazim, W., Mohamed, H. M., and Benmokrane, B. 2020a. Inelastic Second-Order Analysis for Slender GFRP-Reinforced Concrete Columns: Experimental Investigations and Theoretical Study. Journal of Composites for Construction, **24**(3): 04020016.

Abdelazim, W., Mohamed, H. M., Afifi, M. Z., and Benmokrane, B. 2020c. Proposed Slenderness Limit for Glass Fiber-Reinforced Polymer-Reinforced Concrete Columns Based on Experiments and Buckling Analysis. ACI Structural Journal, **117**(1): 241-254.

Abdelazim, W., Mohamed, H. M., Benmokrane, B., and Nolan, S. 2020b. Strength of Bridge High-Strength Concrete Slender Compression Members Reinforced with GFRP Bars and Spirals: Experiments and Second-Order Analysis. Journal of Bridge Engineering, **25**(9): 04020066.

ACI Committee 440. 2015. Guide for the Design and Construction of Structural Concrete Reinforced Fiber-Reinforced Polymer (FRP) Bars (ACI 440.1R-15). American Concrete Institute (ACI), Farmington Hills, Mich.

Afifi, M. Z., Mohamed, H. M., and Benmokrane, B. 2014. Axial Capacity of Circular Concrete Columns Reinforced with GFRP Bars and Spirals. Journal of Composites for Construction, ASCE, **18**(1): 04013017.

Ahmad, A., Elchalakani, M., Elmesalami, N., El Refai, A., and Abed, F. 2021. Reliability Analysis of Strength Models for Short-Concrete Columns under Concentric Loading with FRP Rebars Through Artificial Neural Network. Journal of Building Engineering, **42**: 102497.

Bartlett, F., Hong, H., and Zhou, W. 2003. Load Factor Calibration For The Proposed 2005 Edition of The National Building Code of Canada: Statistics of Loads and Load Effects. Canadian Journal of Civil Engineering, **30**(2): 429-439.

Barua, S., and El-Salakawy, E. 2020. Performance of GFRP-Reinforced Concrete Circular Short Columns under Concentric, Eccentric, and Flexural Loads. Journal of Composites for Construction, **24**(5): 04020044.

Barua, S., Mahmoud, K., and El-Salakawy, E. 2021. Slender GFRP-RC Circular Columns under Concentric, Eccentric, and Flexural Loads: Experimental Investigation. Journal of Bridge Engineering, **26**(7): 04021033.

Commentary to CSA S6. 2019. Canadian Highway Bridge Design Code, Canadian standard association (CSA), Rexdale, Ont.

CSA. 2019. Design of concrete structures. CSA Standard A23.3-19. Canadian standard association (CSA), Rexdale, Ont.

CSA. 2019. Canadian Highway Bridge Design Code. CSA Standard S6-19. Canadian standard association (CSA), Rexdale, Ont.

CSA. 2017. Design and construction of building structures with fibre-reinforced polymers. CSA Standard S806-12. Canadian standard association (CSA), Rexdale, Ont.

Elchalakani, M., and Ma, G. 2017. Tests of Glass Fibre Reinforced Polymer Rectangular Concrete Columns Subjected to Concentric and Eccentric Axial Loading. Engineering Structures, **151**: 93-104.

Elchalakani, M., Dong, M., Karrech, A., Li, G., Mohamed Ali, M. S., and Yang, B. 2019. Experimental Investigation of Rectangular Air-Cured Geopolymer Concrete Columns

Reinforced with GFRP bars and Stirrups. Journal of Composites for Construction, **23**(3): 04019011.

Elchalakani, M., Karrech, A., Dong, M., Ali, M. M., and Yang, B. 2018. Experiments and Finite Element Analysis of GFRP Reinforced Geopolymer Concrete Rectangular Columns Subjected to Concentric and Eccentric Axial Loading. Structures, **14**: 273-289.

Guérin, M., Mohamed, H. M., Benmokrane, B., Nanni, A., and Shield, C. K. 2018a. Eccentric Behavior of Full-Scale Reinforced Concrete Columns with Glass Fiber-Reinforced Polymer Bars and Ties. ACI Structural Journal, **115**(2): 489-499.

Guérin, M., Mohamed, H. M., Benmokrane, B., Shield, C. K., and Nanni, A. 2018b. Effect of Glass Fiber-Reinforced Polymer Reinforcement Ratio on Axial-Flexural Strength of Reinforced Concrete Columns. ACI Structural Journal, **155**(4): 1049-1061.

Hadhood, A., Mohamed, H. M., and Benmokrane, B. 2016. Experimental Study of Circular High-Strength Concrete Columns Reinforced with GFRP Bars and Spirals under Concentric and Eccentric Loading. Journal of Composites for Construction, **21**(2): 04016078.

Hadhood, A., Mohamed, H. M., Ghrib, F., and Benmokrane, B. 2017. Efficiency of Glass-Fiber Reinforced-Polymer (GFRP) Discrete Hoops and Bars in Concrete Columns under Combined Axial and Flexural Loads. Composites Part B: Engineering, **114**: 223-236.

Hadi, M. N., and Youssef, J. 2016. Experimental investigation of GFRP-Reinforced and GFRP-Encased Square Concrete Specimens under Axial and Eccentric Load, and Four-Point Bending Test. Journal of Composites for Construction, **20**(5): 04016020.

Hales, T. A., Pantelides, C. P., and Reaveley, L. D. 2016. Experimental Evaluation of Slender High-Strength Concrete Columns with GFRP and Hybrid Reinforcement. Journal of Composites for Construction, **20**(6): 04016050.

Hasan, H. A., Sheikh, M. N., and Hadi, M. N. 2017. Performance Evaluation of High Strength Concrete and Steel Fibre High Strength Concrete Columns Reinforced with GFRP Bars and Helices. Construction and Building Materials, **134**: 297-310.

Hognestad, E. 1951. A Study of Combined Bending and Axial Load in Reinforced Concrete Members, Bulletin Series No. 399. Urbana: University of Illinois.

Kharal, Z., and Sheikh, S. A. 2020. Seismic Behavior of Square and Circular Concrete Columns with GFRP Reinforcement. Journal of Composites for Construction, **24**(1): 04019059.

Khorramian, K. 2020. Short and Slender Concrete Columns Internally or Externally Reinforced with Longitudinal Fiber-Reinforced Polymer Composites. Halifax, NS, Canada: Ph.D. Thesis, Dalhousie University.

Khorramian, K., and Sadeghian, P. 2017. Experimental and analytical behavior of short concrete columns reinforced with GFRP bars under eccentric loading. Engineering Structures, **151**: 761–773.

Khorramian, K., and Sadeghian, P. 2020. Experimental Investigation of Short and Slender Rectangular Concrete Columns Reinforced with GFRP Bars under Eccentric Axial Loads. Journal of Composites for Construction, **24**(6): 04020072.

Khorramian, K., Oudah, F., and Sadeghian, P. 2021b. Reliability-Based Evaluation of the Stiffness Reduction Factor for Slender GFRP Reinforced Concrete Columns. CSCE Annual Conference. Virtual.

Khorramian, K., Sadeghian, P., and Oudah, F. 2021a. Second-Order Analysis of Slender GFRP Reinforced Concrete Columns using Artificial Neural Network. Virtual: CSCE Annual conference.

Khorramian, K., Sadeghian, P., and Oudah, F. 2021c. Slenderness Limit for GFRP-RC Columns: A Reliability-Based Approach. ACI Structural Journal, Under review.

Kim, J.-K., and Yang, J.-K. 1995. Buckling Behaviour of Slender High-Strength Concrete Columns. Engineering Structures, **17**(1): 39-51.

MacGregor, J. G., and Breen, J. E. 1970. Design of Slender Concrete Columns. Journal Proceedings, **67**(1): 6-28.

Malakzadeh, K., and Daei, M. 2020. Hybrid FORM-Sampling Simulation Method For Finding Design Point and Importance Vector in Structural Reliability. Applied Soft Computing, **92**: 106313.

Mirmiran, A., Yuan, W., and Chen, X. 2001. Design of Slenderness in Concrete Columns Internally Reinforced with Fiber-Reinforced Polymer Bars. ACI Structural Journal, **98**(1): 116-125.

Mohamed, H. M., Afifi, M. Z., and Benmokrane, B. 2014. Performance Evaluation of Concrete Columns Reinforced Longitudinally with FRP Bars and Confined with FRP Hoops and Spirals under Axial Load. Journal of Bridge Engineering, **19**(7): 04014020.

Naderpour, H., Poursaeidi, O., and Ahmadi, M. 2018. Shear Resistance Prediction of Concrete Beams Reinforced by FRP Bars Using Artificial Neural Networks. Measurement, **308**: 299-308.

NBCC. 2015. National Building Code of Canada. National Research Concil. Ottawa, Ont.

Nowak, A. S., and Collins, K. R. 2000. Reliability of structures. McGraw-Hill.

Nowak, A. S., and Szerszen, M. M. 2003. Calibration of Design Code for Buildings (ACI 318): Part 1 — Statistical Models for Resistance. ACI Structural Journal, **100**(3): 377-382.

Oudah, F., El Naggar, M. H., and Norlander, G. 2019. Unified System Reliability Approach For Single and Group Pile Foundations–Theory and Resistance Factor Calibration. Computers and Geotechnics, **108**: 173-182.

Oudah, F., and Hassan, A. 2021. Reliability of Compression-Controlled Flexural FRP Reinforced Concrete Members Designed Using CSA S6, CSA S806, And ACI 440.1R: Comparison and Resistance/Strength Factor Calibration. ACI Special Publication, Under review.

Rackwitz, R., and Flessler, B. 1978. Structural Reliability under Combined Random Load Sequences. Computers and Structures, **9**(5): 489-494.

Raza, A., Shah, S. A., ul Haq, F., Arshad, H., Raza, S. S., Farhan, M., and Waseem, M. 2020. Prediction of Axial Load-Carrying Capacity of GFRP-Reinforced Concrete Columns Through Artificial Neural Networks. Structures, **28**: 1557-1571.

Salah-Eldin, A., Mohamed, H. M., and Benmokrane, B. 2019. Structural Performance of High-Strength-Concrete Columns Reinforced with GFRP Bars and Ties Subjected to Eccentric Loads. Engineering Structures, **185**: 286-300.

Salah-Eldin, A., Mohamed, H. M., and Benmokrane, B. 2020. Effect of GFRP Reinforcement Ratio on the Strength and Effective Stiffness of High-Strength Concrete Columns: Experimental and Analytical Study. Journal of Composites for Construction, **24**(5): 04020055.

Shield, C. K., Galambos, T. V., and Gulbrandsen, P. 2011. On The History and Reliability of The Flexural Strength of FRP Reinforced Concrete Members in ACI 440.1 R. Special Publication, **275**: 1-18.

Sun, L., Wei, M., and Zhang, N. 2017. Experimental Study on The Behavior of GFRP Reinforced Concrete Columns under Eccentric Axial Load. Construction and Building Materials, **152**: 214-225.

Szerszen, M. M., and Nowak, A. S. 2003. Calibration of Design Code for Buildings (ACI 318): Part 2-Reliability Analysis and Resistance Factors. ACI Structural Journal, **100**(3): 383-391.

Tobbi, H., Farghaly, A. S., and Benmokrane, B. 2012. Concrete Columns Reinforced Longitudinally and Transversally with Glass Fiber-Reinforced Polymer Bars. ACI Structural Journal, **109**(4): 551-558.

Xue, W., Peng, F., and Fang, Z. 2018. Behavior and Design of Slender Rectangular Concrete Columns Longitudinally Reinforced with Fiber-Reinforced Polymer Bars. ACI Structural Journal, **115**(2): 311-322.

Zadeh , H. J., and Nanni, A. 2017. Flexural Stiffness and Second-Order Effects in Fiber-Reinforced Polymer-Reinforced Concrete Frames. ACI Structural Journal, **114**(2): 533-543.

Zadeh, H. J., and Nanni, A. 2013. Design of RC Columns Using Glass FRP Reinforcement. Journal of Composites for Construction, **17**(3): 294-304.

Table. 1. Distributions of the studied random variables.

Random variable	Bias	COV	Distribution	Reference
Concrete strength (f_c)	Eq. [*]	0.1	Normal	Nowak and Szerszen (2003)
Yield stress (f_y)	1.145	0.05	Normal	Nowak and Szerszen (2003)
Tensile strength (f_{ftu})	1.15	0.07	Normal	Shield et al. (2011)
Compression strength (f_{fcu})	1	0.13	Lognormal	Khorramian et al. (2021b)
Depth of compressive bars (d_c)	0.99	0.04	Normal	Shield et al. (2011)
Depth of tensile bars (d_t)	0.99	0.04	Normal	Shield et al. (2011)
Dead load (D)*	1.05	0.1	Normal	Bartlett et al. (2003)
Live load (L)*	0.9	0.17	Gumbel	Bartlett et al. (2003)
Transformation to live load effect (LT)*	1	0.206	Normal	Bartlett et al. (2003)
Dead load (D)**	1.04	0.036	Normal	Commentary to CSA S6 (2019)
Live load (L)**	1.168	0.0686	Normal	Commentary to CSA S6 (2019)
Transformation to live load effect (LT)**	1.02	0.09	Normal	Commentary to CSA S6 (2019)
FDM to experimental (ψ_{TE}) for GFRP-RC columns	1.10	0.14	Lognormal	Khorramian et al. (2021c)
FDM to experimental (ψ_{TE}) for steel-RC columns	1.04	0.1	Lognormal	Khorramian et al. (2021c)

Note: COV = coefficient of variation; * = the load statistics used for calibration of steel-RC columns, and GFRP RC columns per CSA S806; ** = the load statistics used for calibration of GFRP-RC columns per CSA S6; Eq. [*] $k_{fc} = -0.0081f_c^3 + 0.1509f_c^2 - 0.9338f_c + 3.0649$ where f_c is the concrete strength in ksi (Nowak and Szerszen 2003).

Table. 2. Design space for reliability analysis.

	GFRP-RC columns		Steel-RC columns	
Parameter	Value	Cases	Value	Cases
End moment ratio (M_1/M_2)	-1, -0.5, 0, +0.5, +1	5	-1, -0.5, 0, +0.5, +1	5
concrete strength (f_c)	20, 40, 60 [MPa]	3	20, 40, 60 [MPa]	3
Reinforcement depth ratio (γ)	0.6, 0.75, 0.9	3	0.6, 0.75, 0.9	3
Steel yield stress (f_y)	-	-	300, 400, 500 [MPa]	3
Reinforcement ratio (ρ)	1, 2, 4 [%]	3	1, 2, 4 [%]	3
GFRP elastic modulus (E_f)	40, 50, 60 [GPa]	3	-	-
Eccentricity ratio (e/h)	0.1, 0.3, 0.5	3	0.1, 0.3, 0.5	3
Slenderness ratio (λ)	14, 17, 20, 22, 24, 27, 30, 33, 37, 40	10	14, 17, 20, 22, 24, 27, 30, 33, 37, 40	10
Dead-to-live load ratio (D/L)	0.25,1, 2, 3, 4, 9, D=0, L=0	8	0.25,1, 2, 3, 4, 9, D=0, L=0	8
GFRP resistance factors (ϕ_f) / Steel resistance factor (ϕ_s)	CSA S806 (0.75), CSA S6 (0.8, 0.65)	3	CSA A23.3 (0.85), CSA S6 (0.85)	2
Total cases	-	291,600	-	194,400

Fig. 1. Analysis: (a) required column analysis; and (b) reliability analysis procedure.

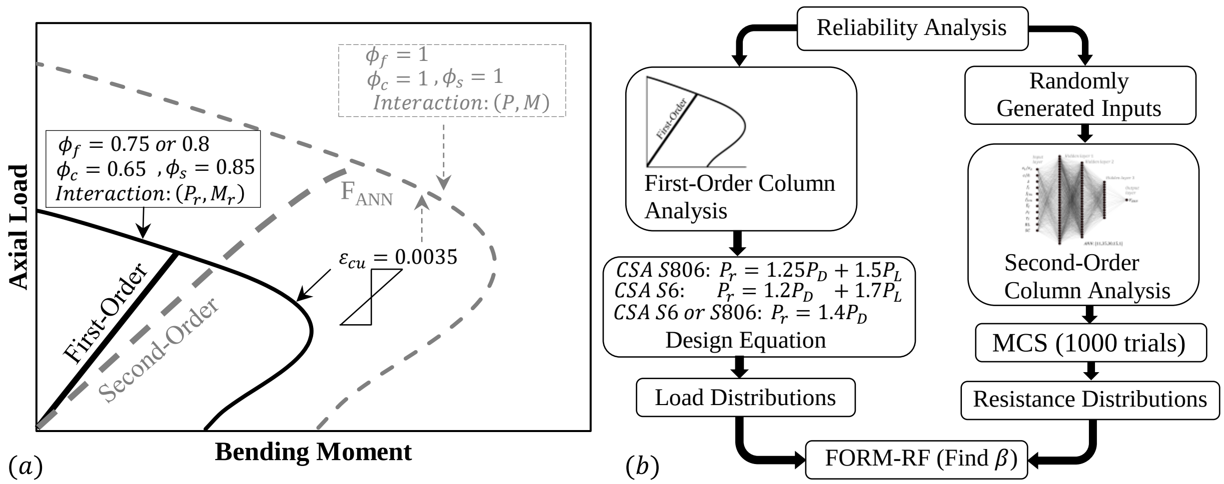

Fig. 2. Parametric study and Reliability analysis results for: (a) parametric study for GFRP-RC columns; (b) parametric study for steel-RC columns; (c) GFRP-RC columns with $\phi_f = 0.75$ for CSA S806; (d) GFRP-RC columns with $\phi_f = 0.80$ for CSA S6; (e) steel-RC columns for CSA S806; and (f) steel-RC columns for CSA S6.

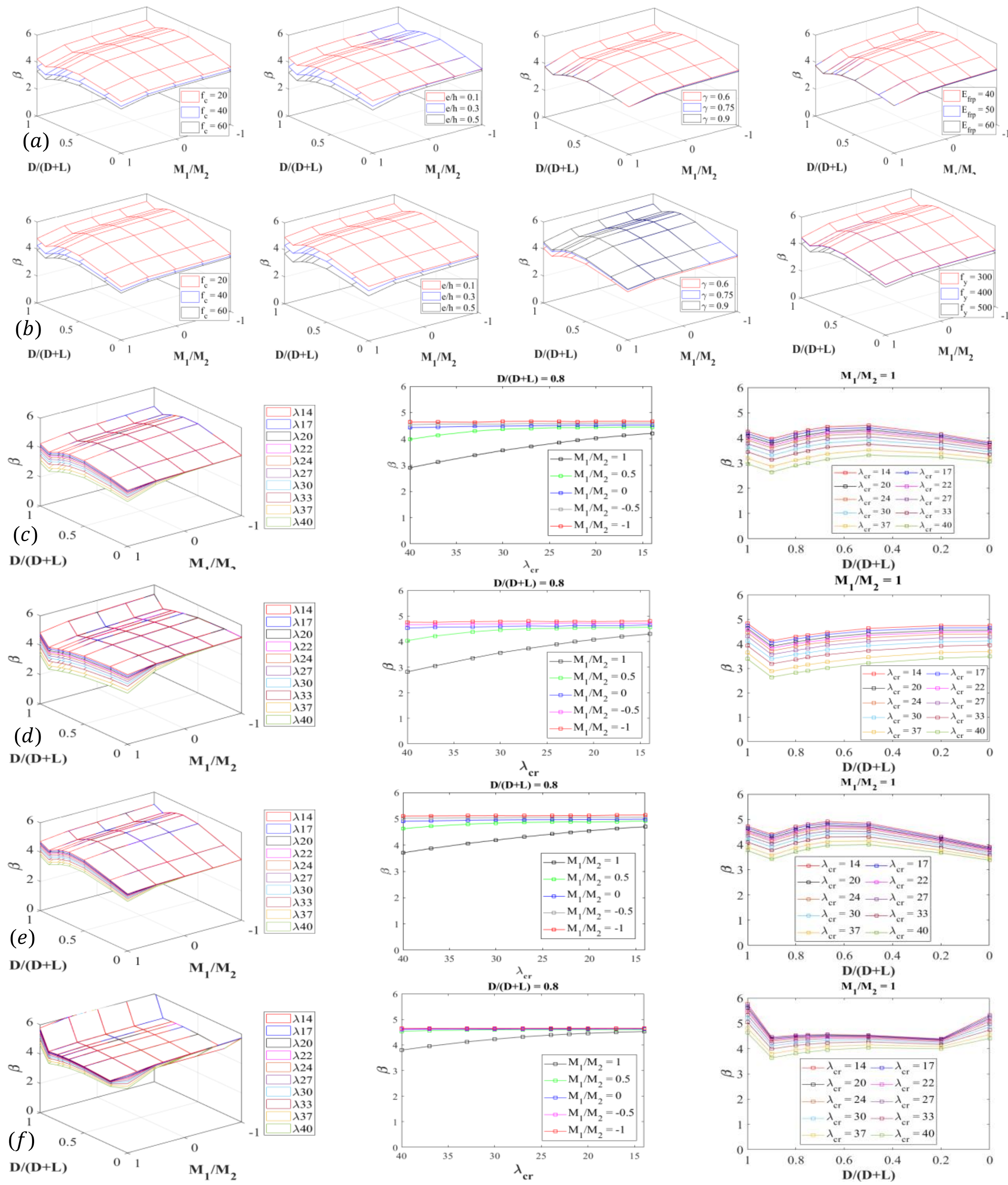

Fig. 3. Code evaluation for steel-RC columns: (a) CSA A23.3-19 (CSA 2019); and (b) CSA S6-19 (CSA 2019).

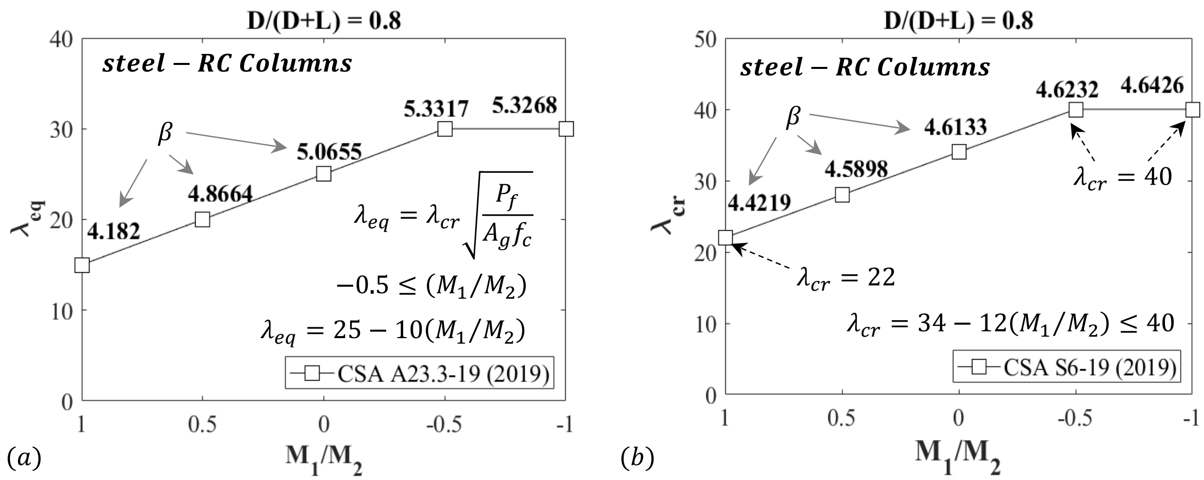

Fig. 4. Code Evaluation and Calibration for GFRP-RC columns: (a) evaluation per CSA S806; (b) proposed for CSA S806; (c) proposed for CSA S6 with ϕ_f = 0.80; and (d) proposed for CSA S6 with ϕ_f = 0.65.